Journal of Computational Physics **182,** 234–261 (2002)
doi:10.1006/jcph.2002.7164

A Dynamic Atomistic–Continuum Method for the Simulation of Crystalline Materials

Weinan E*,† and Zhongyi Huang*,‡

*Department of Mathematics and PACM, Princeton University, Princeton, New Jersey 08544; †School of Mathematics, Peking University, Beijing 100866, China; and ‡Department of Mathematical Sciences, Tsinghua University, Beijing 100084, China
E-mail: weinan@princeton.edu and zhongyih@princeton.edu

Received October 30, 2001; revised June 13, 2002

We present a coupled atomistic–continuum method for the modeling of defects and interface dynamics in crystalline materials. The method uses atomistic models such as molecular dynamics near defects and interfaces, and continuum models away from defects and interfaces. We propose a new class of matching conditions between the atomistic and the continuum regions. These conditions ensure the accurate passage of large-scale information between the atomistic and the continuum regions and at the same time minimize the reflection of phonons at the atomistic–continuum interface. They can be made adaptive by choosing appropriate weight functions. We present applications to dislocation dynamics, friction between two-dimensional crystal surfaces, and fracture dynamics. We compare results of the coupled method and of the detailed atomistic model.

Key Words: atomistic–continuum method; molecular dynamics; dislocation; phonons; friction; crack propagation.

1. INTRODUCTION

Traditionally two apparently separate approaches have been used to model a continuous medium. The first is the continuum theory, in the form of partial differential equations describing the conservation laws and constitutive relations. This approach has been impressively successful in a number of areas, such as solid and fluid mechanics. It is very efficient and simple and often involves very few material parameters. But it becomes inaccurate for problems in which the detailed atomistic processes affect the macroscopic behavior of the medium, or when the scale of the medium is small enough that the continuum approximation becomes questionable. Such situations are often found in studies of properties and defects of micro- or nanosystems and devices. The second approach is atomistic, aiming at finding the detailed behavior of each individual atom using molecular dynamics or quantum

0021-9991/02 $35.00

mechanics. This approach can in principle accurately model the underlying physical processes. But it is often prohibitively expensive.

Recently an alternative approach has been explored that couples the atomistic and continuum approaches [1–7]. The main idea is to use atomistic modeling where the displacement field varies on an atomic scale and to use the continuum approach elsewhere. The most successful and best-known implementation is the quasicontinuum method [1, 2], which combines the adaptive finite element procedure with an atomistic evaluation of the potential energy of the system. This method has been applied to a number of examples [8–10], and interesting details were learned about the structure of crystal defects.

Extension of the quasicontinuum method to dynamic problems has not been straightforward [5–7]. The main difficulty lies in proper matching between the atomistic and the continuum regions. Since the details of the lattice vibrations, the phonons, which are an intrinsic part of the atomistic model, cannot be represented at the continuum level, conditions must be such that the phonons are not reflected at the atomistic–continuum interface. Since the atomistic region is expected to be a very small part of the computational domain, violation of this condition quickly leads to local heating of the atomistic region and destroys the simulation. In addition, the matching at the atomistic–continuum interface must be such that large-scale information is accurately transmitted in both directions.

The main purpose of the present paper is to introduce a new class of matching conditions between atomistic and continuum regions. These matching conditions have the property that they allow accurate passage of large-scale (scales that are represented by the continuum model) information between the atomistic and the continuum regions without reflection of phonon energy to the atomistic region. These conditions can also be used in pure molecular dynamics simulations as border conditions to ensure that there is no reflection of phonons at the boundary of the simulation. As applications, we use our method to study the dynamics of dislocations in the Frenkel–Kontorova model, friction between crystal surfaces, and crack propagation.

2. CONTINUUM APPROXIMATION OF ATOMISTIC MODELS

As a first step toward constructing a coupled atomistic–continuum method, we discuss briefly how continuum equations are obtained from atomistic models.

2.1. 1D Frenkel–Kontorova Model—the Klein–Gordan Equation

We first consider a simple problem, the Frenkel–Kontorova model. This is one-dimensional chain of particles in a periodic potential, coupled by springs. We will take the potential to be

$$U(x) = \frac{1}{2}\mathcal{K}(x - a\,\mathrm{int}(x/a))^2. \tag{2.1}$$

Here a is the equilibrium distance between neighboring particles and $\mathrm{int}(x/a)$ denotes the integer closest to x/a. With the position of the nth particle denoted x_n, the dynamic equation for the particles is given by

$$m\ddot{x}_n = k[x_{n+1} - x_n - a] - k[x_n - x_{n-1} - a] - U'(x_n) + f, \tag{2.2}$$

where f is the applied force.

In the absence of defects such as dislocations, the equilibrium positions of the particles are given by $x_j = ja$. In general, we let $x_j = a(j + u_j)$ and $\tilde{f} = f/a$, where u is the displacement field. We get

$$m\ddot{u}_j = k[u_{j+1} - 2u_j + u_{j-1}] - \mathcal{K}u_j + \tilde{f}. \tag{2.3}$$

Letting $\tau = t\sqrt{1/a^2}$, $\bar{\mathcal{K}} = \mathcal{K}/a^2$, and $\bar{f} = \tilde{f}/a^2$, we obtain

$$m\frac{\partial^2 u_j}{\partial \tau^2} = k\frac{u_{j+1} - 2u_j + u_{j-1}}{a^2} - \bar{\mathcal{K}}u_j + \bar{f}. \tag{2.4}$$

Taking the limit as $a \to 0$, we obtain the continuum limit equation for the displacement field u,

$$m\frac{\partial^2 u}{\partial \tau^2} = k\frac{\partial^2 u}{\partial x^2} - \bar{\mathcal{K}}u + \bar{f}. \tag{2.5}$$

This is simply the Klein–Gordan equation.

One can verify by direct simulation that (2.5) provides a good approximation to (2.2) for small displacements in the absence of defects. However, one interesting aspect of the Frenkel–Kontorova model is the possibility of defects, such as dislocations in the system, which correspond to vacant or doubly occupied potential wells. A dislocation corresponds to a kink in u. In this case the Klein–Gordan equation is no longer a good approximation near the dislocation; we need to couple it with the original Frenkel–Kontorova model in order to accurately model the overall dynamics of the defects as well the displacement field away from the defects.

2.2. 2D Triangular Lattice—Isotropic Elasticity

Next we consider a model for two-dimensional isotropic elasticity. We will assume that nearest-neighbor atoms interact via central forces whose potential is given by $\Phi(r^2)$, where r is the distance between the atoms (see Fig. 1). From Newton's law, we have

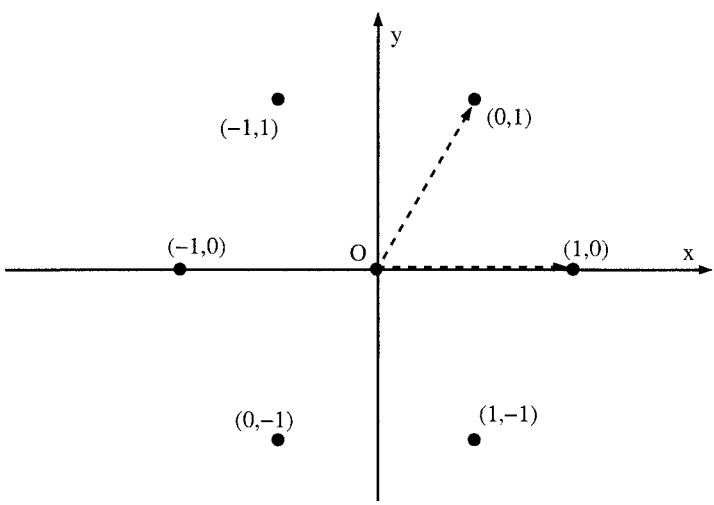

FIG. 1. A triangular lattice.

$$m\ddot{\mathbf{r}}_0 = -\sum_{\mathbf{j}} \nabla_{\mathbf{r}_{0,\mathbf{j}}} \Phi(|\mathbf{r}_{0,\mathbf{j}}|^2), \tag{2.6}$$

where m is the mass of the atoms, $\mathbf{r_j}$ is the position of the $\mathbf{j}$th atom ($\mathbf{j} = (j_1, j_2)$), and $\mathbf{r_{0,j}} = \mathbf{r_0} - \mathbf{r_j}$. Let $\{\mathbf{R_j}\}$ be the equilibrium positions of the atoms. The lattice constant a satisfies the equilibrium condition $\Phi'(a^2) = 0$. Let $\{\mathbf{u_j}\}$ be the displacement vectors, $\mathbf{u_j} = \mathbf{r_j} - \mathbf{R_j}$. Taylor expanding and omitting nonlinear terms in $\mathbf{u}$, we get

$$\begin{aligned} m\ddot{\mathbf{u}}_0 &= -\sum_{\mathbf{j}} \frac{\partial}{\partial |\mathbf{r_{0,j}}|^2} \Phi(|\mathbf{r_{0,j}}|^2) \frac{\partial |\mathbf{r_{0,j}}|^2}{\partial \mathbf{r_{0,j}}} \\ &= -2\sum_{\mathbf{j}} \Phi'(|\mathbf{r_{0,j}}|^2)\mathbf{r_{0,j}} \\ &= -2\sum_{\mathbf{j}} [\Phi'(a^2) + 2\Phi''(a^2)\mathbf{R_j}\cdot(\mathbf{u_j} - \mathbf{u_0})][-\mathbf{R_j} + \mathbf{u_0} - \mathbf{u_j}] \\ &= 4\Phi''(a^2)\sum_{\mathbf{j}} (\mathbf{R_j}\otimes\mathbf{R_j})(\mathbf{u_j} - \mathbf{u_0}). \end{aligned} \tag{2.7}$$

Take the example of a Lennard–Jones potential:

$$\Phi(r) = \epsilon_0\left(\frac{1}{(r/a_0)^{12}} - \frac{1}{(r/a_0)^6}\right). \tag{2.8}$$

The lattice constant a is equal to $2^{1/6}a_0$ under the assumption of nearest-neighbor interaction. In this case, Eq. (2.7) becomes

$$\begin{aligned} \frac{m}{\epsilon_0}\ddot{\mathbf{u}}_0 = \frac{18}{a^2}\Bigg\{ &\begin{pmatrix} 1 & 0 \\ 0 & 0 \end{pmatrix}(\mathbf{u}_{1,0} - 2\mathbf{u}_{0,0} + \mathbf{u}_{-1,0}) + \begin{pmatrix} \frac{1}{4} & \frac{\sqrt{3}}{4} \\ \frac{\sqrt{3}}{4} & \frac{1}{4} \end{pmatrix}(\mathbf{u}_{0,1} - 2\mathbf{u}_{0,0} + \mathbf{u}_{0,-1}) \\ &+ \begin{pmatrix} \frac{1}{4} & -\frac{\sqrt{3}}{4} \\ -\frac{\sqrt{3}}{4} & \frac{1}{4} \end{pmatrix}(\mathbf{u}_{-1,1} - 2\mathbf{u}_{0,0} + \mathbf{u}_{1,-1})\Bigg\}. \end{aligned} \tag{2.9}$$

The continuum limit (as $a \to 0$) of the above equations is

$$\begin{aligned} \frac{m}{\epsilon_0}\frac{\partial^2\mathbf{u}}{\partial\tau^2} &= \begin{pmatrix} 81/4 & 0 \\ 0 & 27/4 \end{pmatrix}\frac{\partial^2\mathbf{u}}{\partial x^2} + \begin{pmatrix} 27/4 & 0 \\ 0 & 81/4 \end{pmatrix}\frac{\partial^2\mathbf{u}}{\partial y^2} + \begin{pmatrix} 0 & 54/4 \\ 54/4 & 0 \end{pmatrix}\frac{\partial^2\mathbf{u}}{\partial x\,\partial y} \\ &= (\lambda + \mu)\nabla(\nabla\cdot u) + \mu\Delta\mathbf{u}, \end{aligned} \tag{2.10}$$

where $\lambda = \mu = \frac{27}{4}$. This is the equation for isotropic elasticity.

2.3. Slepyan Model of Fracture

Here we discuss the one- and two-dimensional Slepyan models of fracture [17]. In the 1D case, one can view it as a model for the atoms lying along a crack surface. Nearest neighbors are connected by elastic springs, with spring constant k, and the atoms are tied to the atoms at the opposite side of the crack surface by similar springs, which, however, snap when extended past some breaking point. The lines of atoms are pulled apart by weak

springs of spring constant k/N. These weak springs are meant schematically to represent N vertical rows of atoms pulling in a series. Let $\{u_{j,+}, u_{j,-}\}$ be the displacement of atoms on the top and bottom crack surfaces, respectively. The equation which describes the upper line of mass points in this model is

$$m\ddot{u}_{j,+} = \begin{cases} k(u_{j+1,+} - 2u_{j,+} + u_{j-1,+}) \\ +\frac{k}{N}(U_N - u_{j,+}) \\ +k(u_{j,-} - u_{j,+})\theta(2u_f - |u_{j,-} - u_{j,+}|) \\ -b\dot{u}_{j,+}. \end{cases} \tag{2.11}$$

Here, the first term at the right hand side is elastic coupling to neighbors. The second term is the driving force, displacing edges of the strip. The third term is the bonding to atoms at the opposite side of the crack surface. The last term is the dissipation, θ is a step function, and the term containing it describes bonds which snap when their total extension reaches the distance $2u_f$. Assume the lattice constant is a. In the region far away from the fracture, we have

$$m\ddot{u}_{j,+} = k(u_{j+1,+} - 2u_{j,+} + u_{j-1,+}) + \frac{k}{N}(U_N - u_{j,+}) + k(u_{j,-} - u_{j,+}) - b\dot{u}_{j,+}. \tag{2.12}$$

Dividing by a^2 and taking the limit as $a \to 0$, we obtain

$$m\frac{\partial^2 u}{\partial \tau^2} = k\frac{\partial^2 u}{\partial x^2} - \tilde{b}\frac{\partial u}{\partial \tau}, \tag{2.13}$$

with $\tau = t\sqrt{1/a^2}$, $\tilde{b} = b/a$.

Now we consider a simple 2D model (see Fig. 2). A crack moves in a lattice strip composed of 2N rows of mass points. Assume that all the atoms are located at square lattice

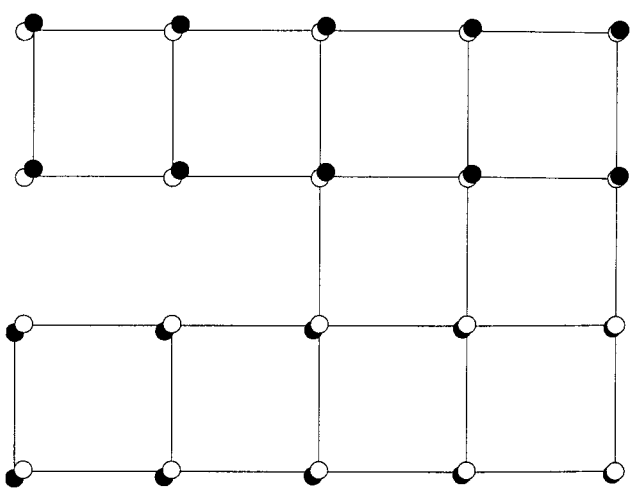

FIG. 2. A 2D Slepyan model of fracture. (White dots) The equilibrium locations; (black dots) the displaced points once stress is applied.

points if there is no exterior force on them. All of the bonds between lattice points behave as perfect linear springs until the instant they snap, at which point they exert no force. The displacement of each mass point is described by a single spatial coordinate $u_{i,j}$, which can be interpreted as the height of mass point (i, j) into or out of the page. The index i takes integer values, while $j = 1/2 - N, \ldots, -1/2, 1/2, \ldots, N - 1/2$. The model is described by the equation

$$m\ddot{u}_{i,j} = -b\dot{u}_{i,j} + \sum_{\substack{\text{nearest} \\ \text{neighbors } (i',j')}} \mathcal{F}(u_{i',j'} - u_{i,j}), \tag{2.14}$$

with

$$\mathcal{F}(r) = kr\theta(2u_f - |r|) \tag{2.15}$$

representing the brittle nature of the springs, and where θ is the step function and b the coefficient of a small dissipative term. The boundary condition which drives the motion of the crack is

$$u_{i,\pm(N-1/2)} = \pm U_N. \tag{2.16}$$

Similarly, we can get the continuum limit of (2.14),

$$m\frac{\partial^2 u}{\partial \tau^2} = k\Delta u - \tilde{b}\frac{\partial u}{\partial \tau}, \tag{2.17}$$

where u is again the displacement field.

3. PHONONS

Among the most essential differences between the atomistic and continuum models is the presence of phonons, the lattice vibrations, at the atomistic scale. In this section we will briefly review the spectrum of the phonons. This will be useful later. Let us first consider the simplest model: 1D discrete wave equation (2.3) with $k = 1$ and $f = 0$. After discretization in time, we have

$$\frac{u_j^{n+1} - 2u_j^n + u_j^{n-1}}{\Delta t^2} = u_{j+1}^n - 2u_j^n + u_{j-1}^n - \mathcal{K}u_j^n, \tag{3.1}$$

where u_j^n is the displacement of the jth particle at time $t = n\Delta t$.

First let $\mathcal{K} = 0$. The phonon spectrum for (3.1) is obtained by looking for solutions of the type $u_j^n = e^{i(n\omega\Delta t + j\xi)}$. This gives us the dispersion relation

$$\frac{1}{\Delta t}\sin\frac{\omega\Delta t}{2} = \sin\frac{\xi}{2}. \tag{3.2}$$

For the case when $\Delta t = 0.01$, this dispersion relation is depicted in Fig. 3. If $\mathcal{K} \neq 0$, we have

$$\frac{1}{\Delta t}\sin\frac{\omega\Delta t}{2} = \sqrt{\sin^2\frac{\xi}{2} + \mathcal{K}/4}. \tag{3.3}$$

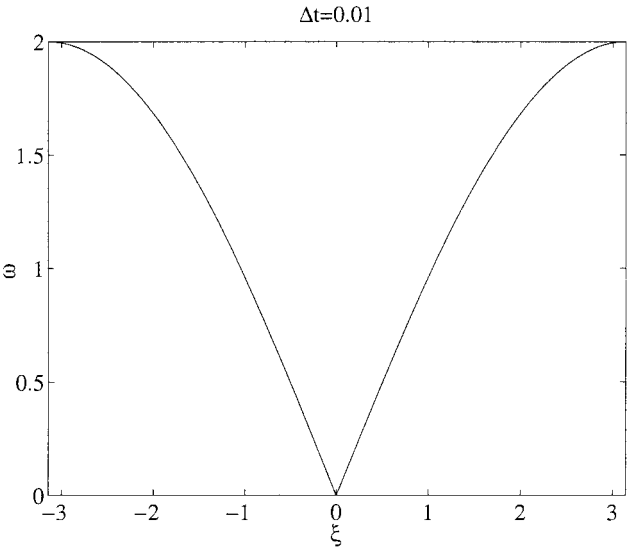

FIG. 3. Dispersion relation.

Consider now the 2D triangular lattice described by (2.7). Let us look for solutions of the type $\mathbf{u}_j^n = e^{i(\xi\cdot\mathbf{r}_j - n\omega\Delta t)}\mathbf{U}$, with $\xi = (\xi_1, \xi_2)^T$. Substituting this expression into (2.7), we obtain

$$\left(\frac{\sin\frac{\omega\Delta t}{2}}{\Delta t/2}\right)^2 \mathbf{U}$$
$$= \frac{18}{a^2}\begin{bmatrix} 4\sin^2\frac{\xi_1 a}{2} + \sin^2\frac{\xi_1+\sqrt{3}\xi_2}{4}a + \sin^2\frac{\xi_1-\sqrt{3}\xi_2}{4}a & \sqrt{3}\left(\sin^2\frac{\xi_1+\sqrt{3}\xi_2}{4}a - \sin^2\frac{\xi_1-\sqrt{3}\xi_2}{4}a\right) \\ \sqrt{3}\left(\sin^2\frac{\xi_1+\sqrt{3}\xi_2}{4}a - \sin^2\frac{\xi_1-\sqrt{3}\xi_2}{4}a\right) & 3\left(\sin^2\frac{\xi_1+\sqrt{3}\xi_2}{4}a + \sin^2\frac{\xi_1-\sqrt{3}\xi_2}{4}a\right) \end{bmatrix}\mathbf{U}$$
$$\equiv \mathbf{A}\mathbf{U}. \tag{3.4}$$

The eigenvalues of the matrix **A** are given by

$$\lambda_\pm = \frac{36}{a^2}\{\alpha+\beta+\gamma \pm \sqrt{\alpha^2+\beta^2+\gamma^2-\alpha\beta-\alpha\gamma-\beta\gamma}\}, \tag{3.5}$$

where

$$\alpha = \sin^2\frac{\xi_1}{2}a, \quad \beta = \sin^2\frac{\xi_1+\sqrt{3}\xi_2}{4}a, \quad \gamma = \sin^2\frac{\xi_1-\sqrt{3}\xi_2}{4}a.$$

The dispersion relation now has two branches,

$$\omega_p(\xi_1,\xi_2) = \frac{2}{\Delta t}\arcsin\left(\frac{2}{\Delta t}\sqrt{\lambda_+}\right), \quad \omega_s(\xi_1,\xi_2) = \frac{2}{\Delta t}\arcsin\left(\frac{2}{\Delta t}\sqrt{\lambda_-}\right), \tag{3.6}$$

where p and s stand for pressure and shear waves, respectively.

4. OPTIMAL LOCAL MATCHING CONDITIONS

We now come to the interface between the atomistic and the continuum regions. As we mentioned earlier, designing proper matching conditions at this interface is a major challenge in such a coupled atomistic–continuum approach. The basic requirements for the matching conditions are the following:

1. Reflection of phonons to the atomistic region should be minimal. This is particularly crucial since the atomistic regions are typically very small for the purpose of computational efficiency, and reflection of phonon energy back to the atomistic region will trigger local heating and melt the crystalline structure.
2. There should be accurate exchange of large-scale information between the atomistic and the continuum regions.

The first requirement is reminiscent of the absorbing boundary conditions required for the computation of waves [13, 14]. Indeed our work draws much inspiration from that literature. There are some crucial differences though between the phonon problem considered here and the ones studied in [13, 14]. The most obvious one is the fact that electromagnetic and acoustic waves are continuum objects modeled by partial differential equations, and the associated absorbing boundary conditions often use small wavenumber and/or frequency approximations, whereas phonons are intrinsically discrete, with substantial energy distributed at high wavenumbers.

In the following we will give an example of a simple discrete wave equation for which exact reflectionless boundary conditions can be found. Such exact boundary conditions are highly nonlocal and therefore not practical. But they give us guidelines on how approximate boundary conditions should be constructed. We then present a method that constructs optimal local matching conditions, given a predetermined stencil.

4.1. Exact Boundary Conditions for 1D Discrete Wave Equation

Consider Eq. (3.1). It is supposed to be solved for all integer values of j. Now let us assume that we will truncate the computational domain and only compute u_j^n for $j \geq 0$. Assuming there are no sources of waves coming from $j < 0$, we still want to obtain the same solution as when the computation is done for all j. At $j = 0$, we will impose a new boundary condition to make sure that the phonons arriving from $j > 0$ are not reflected back at $j = 0$.

At $j = 0$, we replace (3.1) with

$$u_0^n = \sum_{k,j\geq 0} a_{k,j} u_j^{n-k}, \quad a_{0,0} = 0. \tag{4.1}$$

We would like to determine the coefficients $\{a_{k,j}\}$. For the simple problem at hand, it is possible to obtain analytical formulas of $\{a_{k,j}\}$ such that the imposition of (4.1) together with the solution of (3.1) for $j > 0$ reproduces exactly the solution of (3.1) when solved for all integer values of j; i.e., an exact reflectionless boundary condition can be found. (For a review on discrete transparent boundary conditions, see [12]).

First, let us consider the case of $\mathcal{K} = 0$. Let $\lambda = \Delta t$ and let us look for solutions of the form

$$u_j^n = z^n \xi^j, \quad |\xi| \leq 1. \tag{4.2}$$

Substituting (4.2) into (3.1), we get

$$\frac{1}{\lambda^2}\left(z-2+\frac{1}{z}\right)=\xi-2+\frac{1}{\xi}. \tag{4.3}$$

This equation has two roots for ξ:

$$\xi_{1,2}=1+\frac{z^2-2z+1}{2\lambda^2 z}\pm\frac{1}{2\lambda^2 z}\sqrt{(z-1)^2[z^2+(4\lambda^2-2)z+1]}. \tag{4.4}$$

Assume a boundary condition of the form

$$u_0^{n+1}=2u_0^n-u_0^{n-1}+\lambda^2\left(u_1^n-2u_0^n\right)+\sum_{k=1}^{n}s_k u_0^{n-k}. \tag{4.5}$$

Substituting (4.2) into (4.5), we get

$$z-2+\frac{1}{z}-\lambda^2\left(\frac{1}{\xi}-2\right)=\sum_{k=1}^{n}s_k z^{-k}.$$

To find s_k, we have to find the Laurent expansion of the function on the left hand side. Let

$$H(z)=\sqrt{(z-1)^2[z^2+(4\lambda^2-2)z+1]}. \tag{4.6}$$

Observe that $H(z)$ satisfies

$$H'(z)=2(z-1)[z^2+(3\lambda^2-2)z+1-\lambda^2]/H(z).$$

Hence

$$H'(z)\cdot\{(z-1)[z^2+(4\lambda^2-2)z+1]\}=2(z-1)[z^2+(3\lambda^2-2)z+1-\lambda^2]H(z). \tag{4.7}$$

Solving this equation using a Laurent series, $H(z)=\sum_{m\geq -2}\mu_m z^{-m}$, we obtain a recursion relation μ_m for $m\geq 1$,

$$\begin{aligned}(m+2)\mu_m=&[1-2\lambda^2-m(4\lambda^2-3)]\mu_{m-1}\\&+[4-6\lambda^2-m(3-4\lambda^2)]\mu_{m-2}+(m-3)\mu_{m-3},\end{aligned} \tag{4.8}$$

and

$$\mu_{-2}=1,\quad \mu_{-1}=2\lambda^2-2,\quad \mu_0=1-2\lambda^4. \tag{4.9}$$

Then from (4.4)–(4.9), we have

$$s_1=\lambda^4,\quad s_k=-\frac{\mu_{k-1}}{2},\quad \text{for } k\geq 2. \tag{4.10}$$

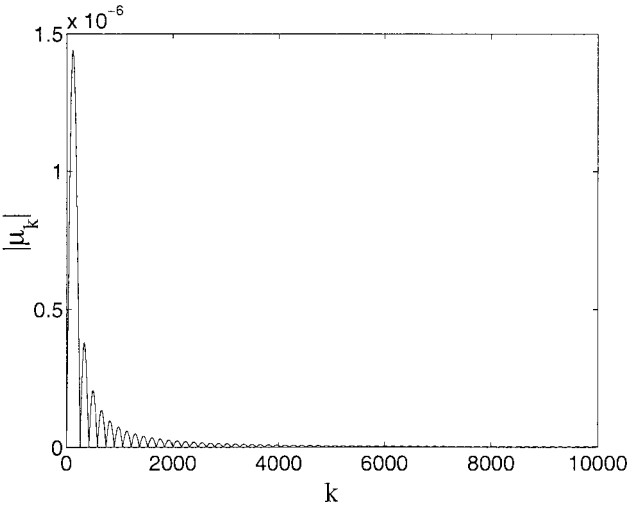

FIG. 4. The decay tendency of $|\mu_k|$.

Equation (4.5) is nonlocal and has memory effects. In order to see how fast the memory decays, let us assume $\mu_k \sim m^\alpha$ when $m \gg 1$. Substituting into (4.8), and equating the coefficients of term order m^α, we get

$$2 = (4\lambda^2 - 3)(1+\alpha) + (4 - 6\lambda^2) + 2(3 - 4\lambda^2)(1+\alpha) + (2\lambda^2 - 2) - 3(1+\alpha).$$

This gives $\alpha = -2$. The behavior of μ_k when $\lambda = 0.01$ is shown in Fig. 4.

If $\mathcal{K} \neq 0$, we can proceed as before. But (4.4) changes to

$$\xi_{1,2} = 1 + \frac{\mathcal{K}}{2} + \frac{z^2 - 2z + 1}{2\lambda^2 z} \pm \frac{1}{2\lambda^2 z}\sqrt{[z^2 + (\mathcal{K}\lambda^2 - 2)z + 1][z^2 + (\mathcal{K}\lambda^2 + 4\lambda^2 - 2)z + 1]}. \quad (4.11)$$

Assuming a boundary condition of the form

$$u_0^{n+1} = 2u_0^n - u_0^{n-1} + \lambda^2\left[u_1^n - (2 + \mathcal{K})u_0^n\right] + \sum_{k=0}^{n} s_k u_0^{n-k}, \quad (4.12)$$

substituting (4.2) into (4.12), we get

$$z - 2 + \frac{1}{z} - \lambda^2\left(\frac{1}{\xi} - 2 - \mathcal{K}\right) = \sum_{k=1}^{n} s_k z^{-k}.$$

To find the Laurent expansion of the function on the left hand side, let $g(\mathcal{K}, \lambda) = \mathcal{K}\lambda^2 + 2\lambda^2 - 2$ and

$$H(z) = \sqrt{[z^2 + (\mathcal{K}\lambda^2 - 2)z + 1][z^2 + (\mathcal{K}\lambda^2 + 4\lambda^2 - 2)z + 1]}. \quad (4.13)$$

Observe that $H(z)$ satisfies

$$H'(z) = \{2z^3 + 3g(\mathcal{K}, \lambda)z^2 + [g^2(\mathcal{K}, \lambda) + 2 - 4\lambda^4]z + g(\mathcal{K}, \lambda)\}/H(z).$$

Hence

$$\begin{aligned} &H'(z) \cdot \{z^4 + 2g(\mathcal{K}, \lambda)z^3 + [g^2(\mathcal{K}, \lambda) + 2 - 4\lambda^4]z^2 + 2g(\mathcal{K}, \lambda)z + 1\} \\ &\quad = H(z) \cdot \{2z^3 + 3g(\mathcal{K}, \lambda)z^2 + [g^2(\mathcal{K}, \lambda) + 2 - 4\lambda^4]z + g(\mathcal{K}, \lambda)\}. \end{aligned} \tag{4.14}$$

Solving this equation using a Laurent series, $H(z) = \sum_{m \geq -2} \mu_m z^{-m}$, we obtain a recursion relation μ_m for $m \geq 2$,

$$\begin{aligned} (m+2)\mu_m = {} & (2m+1)[2 - \lambda^2(\mathcal{K}+2)]\mu_{m-1} + (1-m)\{2 - 4\lambda^4 + [2 - \lambda^2(\mathcal{K}+2)]^2\}\mu_{m-2} \\ & + (2 - \mathcal{K}\lambda^2 - 2\lambda^2)(2m-5)\mu_{m-3} + (4-m)\mu_{m-4}, \end{aligned} \tag{4.15}$$

and

$$\mu_{-2} = 1, \quad \mu_{-1} = \mathcal{K}\lambda^2 + 2\lambda^2 - 2, \quad \mu_0 = 1 - 2\lambda^4, \quad \mu_1 = 2\lambda^4(\mathcal{K}\lambda^2 + 2\lambda^2 - 2). \tag{4.16}$$

Then from (4.11)–(4.16), we have

$$s_0 = -\lambda^2\mathcal{K}, \quad s_1 = \lambda^4, \quad s_k = -\frac{\mu_{k-1}}{2}, \quad \text{for } k \geq 2. \tag{4.17}$$

In order to see how fast the memory decays, let us assume $\mu_k \sim m^\alpha$ when $m \gg 1$. Substituting it into (4.15), and equating the coefficients of the term $m^{\alpha-1}$, we get

$$0 = \alpha\{g(\mathcal{K}, \lambda)(2-\alpha) - 2\alpha[g^2(\mathcal{K}, \lambda) + 2 - 4\lambda^2] - (6 + 9\alpha)g(\mathcal{K}, \lambda) - 8 - 8\alpha\}.$$

This gives $\alpha = 0$ or $\alpha = -2/\{1 + \frac{\mathcal{K}(\mathcal{K}+4)}{\mathcal{K}+2}\lambda^2\}$.

These exact boundary conditions should be the same as the ones found numerically in [7]. It represents the exact Green's function for (3.1), which is nonlocal. However, such boundary conditions appear to be impractical for realistic models since they are nonlocal and difficult to obtain, particularly when the atomistic region moves with time, which is the case that interests us. But such calculations can at least give us guidelines on how to construct approximately reflectionless boundary conditions.

4.2. Optimal Local Matching Conditions for 1D Discrete Wave Equation

A practical solution is to restrict (4.1) to a finite number of terms and look for the coefficients $\{a_{k,j}\}$ that minimize reflection. In order to do this, let us look for solutions of the type

$$u_j^n = e^{i(n\omega\Delta t + j\xi)} + R(\xi)e^{i(n\omega\Delta t - j\xi)}, \tag{4.18}$$

where ω is given by (3.2). $R(\xi)$ is the reflection coefficient at wavenumber ξ. Inserting (4.18) into (4.1), we obtain

$$R(\xi) = -\frac{\sum a_{k,j} e^{i(j\xi - k\omega\Delta t)} - 1}{\sum a_{k,j} e^{-i(j\xi + k\omega\Delta t)} - 1}. \tag{4.19}$$

Our goal is to find $\{a_{k,j}\}$ in order to do the following:

1. Minimize total reflection.
2. Guarantee accuracy at large scales.

One way of achieving this is to require $\{a_{k,j}\}$ to satisfy

$$\min \int_0^\pi W(\xi)|R(\xi)|^2\,d\xi \tag{4.20}$$

subject to the constraint

$$R(0) = 0, \quad R'(0) = 0, \text{ etc.} \tag{4.21}$$

Here $W(\xi)$ is a weight function, which is chosen to be $W(\xi) = 1$ in the examples below. Condition (4.21) guarantees accuracy at large scales and (4.20) guarantees that the total amount of reflection is minimized. This procedure offers a lot of flexibility. For example, instead of $\int_0^\pi |R(\xi)|^2\,d\xi$, we can minimize the total reflection over certain carefully selected intervals. Another possibility is to choose the weight function to be the (empirically computed) energy spectrum. The coefficients $\{a_{k,j}\}$ may then change in time to reflect the change in the nature of the small scales. In practice, we found it preferable to use $\int_0^{\pi-\delta} |R(\xi)|^2\,d\xi$ with some small δ, instead of $\int_0^\pi |R(\xi)|^2\,d\xi$, in order to minimize the influence of $\xi = \pi$, which always satisfies $R(\pi) = 1$.

Let us look at a few examples. If in (4.1) we only keep the terms involving $a_{1,0}$ and $a_{1,1}$, then imposing the condition $R(0) = 0$ gives

$$u_0^n = (1 - \Delta t)u_0^{n-1} + \Delta t u_1^{n-1}. \tag{4.22}$$

If instead we keep terms involving $a_{0,1}$, $a_{1,0}$, and $a_{1,1}$, we can then impose both $R(0) = 0$ and $R'(0) = 0$. This gives us

$$u_0^n = u_1^{n-1} + \frac{1 - \Delta t}{1 + \Delta t}\left(u_0^{n-1} - u_1^n\right). \tag{4.23}$$

Conditions of the type (4.22) and (4.23) are intimately related to the absorbing boundary conditions proposed and analyzed in [13, 14] for the computation of waves. These conditions perform well for low wavenumbers but are less satisfactory at high wavenumbers.

To improve the performance at high wavenumbers let us consider a case that includes all terms with $k \le 2$, $j \le 3$ and minimizes $\int_0^{\pi-\delta} |R(\xi)|^2\,d\xi$ (with $\delta = 0.125\pi$) subject to the condition $R(0) = 0$. The optimal coefficients can be easily found numerically and are given by

$$(a_{k,j}) = \begin{pmatrix} 1.95264 & -7.4207 \times 10^{-2} & -1.4903 \times 10^{-2} \\ -0.95406 & 7.4904 \times 10^{-2} & 1.5621 \times 10^{-2} \end{pmatrix}. \tag{4.24}$$

If instead we only include all terms such that $k \le 3$, $j \le 2$, then

$$(a_{k,j}) = \begin{pmatrix} 2.9524 & 1.5150 \times 10^{-2} \\ -2.9065 & -3.0741 \times 10^{-2} \\ 0.95406 & 1.5624 \times 10^{-2} \end{pmatrix}. \tag{4.25}$$

The resulting reflection coefficients R are displayed in Fig. 5.

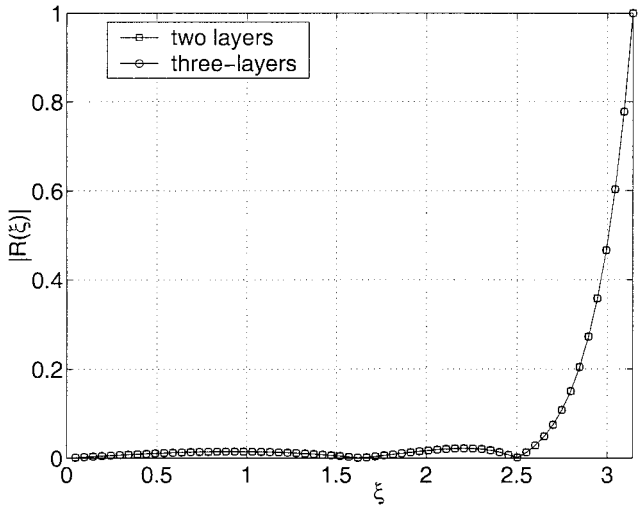

FIG. 5. Reflection coefficients for (4.24) and (4.25).

4.3. Optimal Local Matching Conditions for Triangular Lattice

The above procedure can be easily generalized. Let us take the triangular lattice as an example, with the boundary along the x-axis. Given a boundary condition of the form

$$u_0^{n+1} = \sum_{l \le 1} \sum_{\mathbf{j}} \mathbf{A}_{\mathbf{j}}^l \mathbf{u}_{\mathbf{j}}^{n+l}, \tag{4.26}$$

where $\mathbf{A}_{\mathbf{j}}^l$ are 2×2 matrices ($\mathbf{A}_0^1 = 0$) and the summation is done over a preselected stencil, we can find the reflection matrix associated with this boundary condition. For that purpose, we look for solutions of the form

$$\mathbf{u}_{\mathbf{j}}^n = \sum_{\alpha = I, O} \sum_{\beta = s, p} C_\beta^\alpha e^{i(\xi^{\alpha\beta} \cdot \mathbf{r}_{\mathbf{j}} - \omega t)} \mathbf{U}_\beta^\alpha, \tag{4.27}$$

where $\alpha = I, O$ corresponds to incoming and outgoing waves, respectively (see Fig. 6),

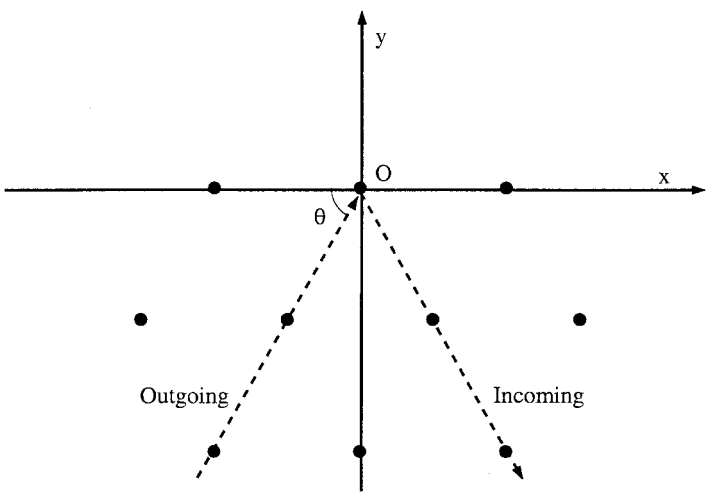

FIG. 6. The incoming and outgoing phonons near the boundary.

and $\beta = s, p$ corresponds to shear and pressure waves, respectively. Substituting into (3.4) we obtain a relation between $(C_s^O, C_p^O)^T$ and $(C_s^I, C_p^I)^T$,

$$\mathbf{M}_O \begin{pmatrix} C_s^O \\ C_p^O \end{pmatrix} = \mathbf{M}_I \begin{pmatrix} C_s^I \\ C_p^I \end{pmatrix}, \tag{4.28}$$

where

$$\mathbf{M}_O = e^{-i\omega\Delta t}\left[U_s^O, U_p^O\right] - \sum_{l\le 1}\sum_{\mathbf{j}} \mathbf{A}_{\mathbf{j}}^l \left[e^{i(\xi^{Os}\cdot \mathbf{r}_{\mathbf{j}} - l\omega\Delta t)} U_s^O, e^{i(\xi^{Op}\cdot \mathbf{r}_{\mathbf{j}} - l\omega\Delta t)} U_p^O\right], \tag{4.29}$$

$$\mathbf{M}_I = -e^{-i\omega\Delta t}\left[U_s^I, U_p^I\right] + \sum_{l\le 1}\sum_{\mathbf{j}} \mathbf{A}_{\mathbf{j}}^l \left[e^{i(\xi^{Is}\cdot \mathbf{r}_{\mathbf{j}} - l\omega\Delta t)} U_s^I, e^{i(\xi^{Ip}\cdot \mathbf{r}_{\mathbf{j}} - l\omega\Delta t)} U_p^I\right]. \tag{4.30}$$

In principle, we can solve the minimization problem

$$\min \int W(\xi)\left\|\mathbf{M}_I^{-1}\cdot \mathbf{M}_O(\xi)\right\|^2 d\xi \tag{4.31}$$

to find optimal $\{\mathbf{A}_{\mathbf{j}}^l\}$, where the integration is over the Brillion zone. But in practice, we find it much more convenient to restrict the integration over a few selected low-symmetry atomic planes. In the present context, it amounts to choosing special incidences where the phonon energy dominates.

First, let us consider the case of normal incidence $\theta = 90^\circ$. That means $\xi_1 = 0$. Then the matrix $\mathbf{A}$ in (3.4) becomes a diagonal matrix,

$$\mathbf{A} = \frac{18}{a^2}\begin{bmatrix} 2\sin^2\frac{\sqrt{3}\xi_2 a}{4} & 0 \\ 0 & 6\sin^2\frac{\sqrt{3}\xi_2 a}{4} \end{bmatrix},$$

with eigenvalues and eigenvectors

$$\lambda_1 = \frac{36}{a^2}\sin^2\frac{\sqrt{3}\xi_2 a}{4}, \quad \mathbf{U}_1 = (1,0)^T,$$

$$\lambda^2 = \frac{108}{a^2}\sin^2\frac{\sqrt{3}\xi_2 a}{4}, \quad \mathbf{U}_2 = (0,1)^T.$$

The dispersion relations are

$$\omega_s\Delta t = 2\arcsin\left(\frac{3\Delta t}{a}\sin\frac{\sqrt{3}\xi_2 a}{4}\right), \qquad \mathbf{U}_s = (1,0)^T, \tag{4.32}$$

$$\omega_p\Delta t = 2\arcsin\left(\frac{3\sqrt{3}\Delta t}{a}\sin\frac{\sqrt{3}\xi_2 a}{4}\right), \quad \mathbf{U}_p = (0,1)^T. \tag{4.33}$$

If we take the boundary condition as in (4.26), the matrices $\mathbf{M}_O$ and $\mathbf{M}_I$ are given by

$$\mathbf{M}_O = e^{-i\omega\Delta t} I - \sum_{l\le 1}\sum_{\mathbf{j}} \mathbf{A}_{\mathbf{j}}^l \begin{pmatrix} e^{i(\xi_2^{Os} y_{\mathbf{j}} - l\omega\Delta t)} & 0 \\ 0 & e^{i(\xi_2^{Op} y_{\mathbf{j}} - l\omega\Delta t)} \end{pmatrix}, \tag{4.34}$$

$$\mathbf{M}_I = -e^{-i\omega\Delta t} I + \sum_{l\le 1}\sum_{\mathbf{j}} \mathbf{A}_{\mathbf{j}}^l \begin{pmatrix} e^{i(\xi_2^{I^s} y_{\mathrm{j}} - l\omega\Delta t)} & 0 \\ 0 & e^{i(\xi_2^{I^p} y_{\mathrm{j}} - l\omega\Delta t)} \end{pmatrix}, \tag{4.35}$$

where I is the 2×2 identity matrix. For consistency, we should require that

$$\big(\mathbf{M}_I^{-1}\mathbf{M}_O\big)(0) = 0.$$

Imposing this, we get

$$I = \sum_{l\le 1}\sum_{\mathbf{j}} \mathbf{A}_{\mathbf{j}}^l, \tag{4.36}$$

$$0 = \Delta t I + \sum_{l\le 1}\sum_{\mathbf{j}} \mathbf{A}_{\mathbf{j}}^l \begin{pmatrix} \frac{2\sqrt{3}a}{9} y_{\mathrm{j}} - l\Delta t & 0 \\ 0 & \frac{2a}{9} y_{\mathrm{j}} - l\Delta t \end{pmatrix}. \tag{4.37}$$

If we minimize (4.31) along normal incidence subject to the constraints (4.36) and (4.37), we obtain the desired matrices $\mathbf{A}_{\mathbf{j}}^l$. For example, if we keep the terms with $l = 0$, 1 and $\mathbf{j} = (0,0), (-1,0), (-1,1)$, the optimal coefficient matrices are

$$\mathbf{A}_{(0,0)}^0 = \begin{pmatrix} 0.947937634 & -0.423061769E-09 \\ -0.411523005E-09 & 0.911511476 \end{pmatrix},$$

$$\mathbf{A}_{(-1,0)}^0 = \mathbf{A}_{(-1,1)}^0 = \begin{pmatrix} 0.500000011 & 0.604865049E-08 \\ 0.105260341E-07 & 0.499999996 \end{pmatrix},$$

$$\mathbf{A}_{(-1,0)}^1 = \mathbf{A}_{(-1,1)}^1 = \begin{pmatrix} -0.473968784 & -0.603638049E-08 \\ -0.102331855E-07 & -0.455755718 \end{pmatrix}.$$

Next we consider the cases when both $\theta = 60^\circ$ and $\theta = 120^\circ$ are taken into account. For $\theta = 60^\circ$, we have $\xi_2 = \sqrt{3}\xi_1$, and

$$\mathbf{A} = \frac{18}{a^2}\sin^2\frac{\xi_1 a}{2}\begin{bmatrix} 9 - 4\sin^2\frac{\xi_1 a}{2} & \sqrt{3}\big(3 - 4\sin^2\frac{\xi_1 a}{2}\big) \\ \sqrt{3}\big(3 - 4\sin^2\frac{\xi_1 a}{2}\big) & 15 - 12\sin^2\frac{\xi_1 a}{2} \end{bmatrix},$$

with two eigenvalues and eigenvectors,

$$\lambda_1 = \frac{108}{a^2}\sin^2\frac{\xi_1 a}{2}, \qquad \mathbf{U}_1 = (\sqrt{3}, -1)^T,$$

$$\lambda_2 = \frac{36}{a^2}\sin^2\frac{\xi_1 a}{2}\left(9 - 8\sin^2\frac{\xi_1 a}{2}\right), \quad \mathbf{U}_2 = (1, \sqrt{3})^T.$$

The dispersion relations are

$$\omega_s\Delta t = 2\arcsin\left(\frac{3\sqrt{3}\Delta t}{a}\sin\frac{\xi_1^s a}{2}\right), \qquad \mathbf{U}_s = (\sqrt{3}, -1)^T, \tag{4.38}$$

$$\omega_p\Delta t = 2\arcsin\left(\frac{3\Delta t}{a}\sin\frac{\xi_1^p a}{2}\sqrt{9 - 8\sin^2\frac{\xi_1^p a}{2}}\right), \quad \mathbf{U}_p = (1, \sqrt{3})^T. \tag{4.39}$$

The consistency constraints are

$$I = \sum_{l\le 1}\sum_{\mathbf{j}} \mathbf{A}^l_{\mathbf{j}}, \tag{4.40}$$

$$0 = \Delta t \begin{pmatrix} \sqrt{3} & 1 \\ -1 & \sqrt{3} \end{pmatrix} + \sum_{l\le 1}\sum_{\mathbf{j}} \mathbf{A}^l_{\mathbf{j}} \begin{pmatrix} \sqrt{3}(\xi^{Is}\cdot \mathbf{r}_{\mathbf{j}}/\omega - l\Delta t) & \xi^{Ip}\cdot \mathbf{r}_{\mathbf{j}}/\omega - l\Delta t \\ -(\xi^{Is}\cdot \mathbf{r}_{\mathbf{j}}/\omega - l\Delta t) & \sqrt{3}(\xi^{Ip}\cdot \mathbf{r}_{\mathbf{j}}/\omega - l\Delta t) \end{pmatrix} \tag{4.41}$$

for $\theta = 60^\circ$, and

$$I = \sum_{l\le 1}\sum_{\mathbf{j}} \mathbf{A}^l_{\mathbf{j}}, \tag{4.42}$$

$$0 = \Delta t \begin{pmatrix} \sqrt{3} & -1 \\ 1 & \sqrt{3} \end{pmatrix} + \sum_{l\le 1}\sum_{\mathbf{j}} \mathbf{A}^l_{\mathbf{j}} \begin{pmatrix} \sqrt{3}(\xi^{Is}\cdot \mathbf{r}_{\mathbf{j}}/\omega - l\Delta t) & -(\xi^{Ip}\cdot \mathbf{r}_{\mathbf{j}}/\omega - l\Delta t) \\ \xi^{Is}\cdot \mathbf{r}_{\mathbf{j}}/\omega - l\Delta t & \sqrt{3}(\xi^{Ip}\cdot \mathbf{r}_{\mathbf{j}}/\omega - l\Delta t) \end{pmatrix} \tag{4.43}$$

for $\theta = 120^\circ$. For example, if we keep the terms for $l = 0, 1$ and $\mathbf{j} = (0,0), (-1,0), (-1,1)$, we have the optimal coefficient matrices

$$\mathbf{A}^0_{(0,0)} = \begin{pmatrix} 0.929252841 & -0.861918368E-09 \\ 0.355336047E-09 & 0.908823412 \end{pmatrix},$$

$$\mathbf{A}^0_{(-1,0)} = \begin{pmatrix} 0.504255087 & 0.156041692E-01 \\ 0.161793547E-01 & 0.499201553 \end{pmatrix},$$

$$\mathbf{A}^0_{(-1,1)} = \begin{pmatrix} 0.504255087 & -0.156041692E-01 \\ -0.161793547E-01 & 0.499201553 \end{pmatrix},$$

$$\mathbf{A}^1_{(-1,0)} = \begin{pmatrix} -0.468881506 & 0.128308044E-01 \\ 0.118075167E-01 & -0.453613259 \end{pmatrix},$$

$$\mathbf{A}^1_{(-1,1)} = \begin{pmatrix} -0.468881506 & -0.128308044E-01 \\ -0.118075167E-01 & -0.453613259 \end{pmatrix}.$$

If all three angles $\theta = 60^\circ, 90^\circ$, and 120° are used with equal weight, then the optimal coefficient matrices are given by

$$\mathbf{A}^0_{(0,0)} = \begin{pmatrix} 0.963685659E+00 & 0.522045701E-05 \\ 0.186532512E-05 & 0.911580620E+00 \end{pmatrix},$$

$$\mathbf{A}^0_{(-1,0)} = \begin{pmatrix} 0.190155146E+00 & 0.439544149E-02 \\ 0.132862553E-01 & 0.497292487E+00 \end{pmatrix},$$

$$\mathbf{A}^0_{(-1,1)} = \begin{pmatrix} 0.190158427E+00 & -0.439289996E-02 \\ -0.132859770E-01 & 0.497292916E+00 \end{pmatrix},$$

$$\mathbf{A}^0_{(-1,0)} = \begin{pmatrix} -0.171943945E+00 & 0.439598834E-02 \\ 0.132858254E-01 & -0.459575584E+00 \end{pmatrix},$$

$$\mathbf{A}^1_{(-1,1)} = \begin{pmatrix} -0.171944818E+00 & -0.439293875E-02 \\ -0.132856732E-01 & -0.453075576E+00 \end{pmatrix}.$$

5. THE OVERALL ALGORITHM

Now we are ready to describe our overall coupled atomistic–continuum method. Our main objective is to accurately model the macroscopic behavior of the system, not the microscopic details. Therefore we will base our computation on a macroscopic grid, with grid sizes denoted Δt and Δx. The computational domain is divided into two nonoverlapping continuum and atomistic regions. This division is done adaptively during the computation, as we explain below. In the continuum region, we solve the linear elasticity equation using conventional finite difference methods. In the atomistic region, we also evolve the macroscopic variables, but with elastic forces computed through averaging the result of the atomistic model.

Each macro time step involves solving a subproblem using the atomistic model in the atomistic region. This micro subproblem is solved via the following steps.

1. Obtain the initial data inside the atomistic region for the atomistic model by interpolating the macroscopic data.
2. Evolve the atomistic model in the atomistic region using the boundary conditions discussed in the last section.
3. Evaluate the macroscopic elastic forces in the atomistic region by averaging the results from the atomistic model.

In the current implementation, for which no coarse graining in time is used, step 1 is only necessary when a macro cell is changed from a continuum cell to an atomistic cell.

At each macro step the overall scheme consists of the following:

(i) Selecting the atomistic and the continuum regions, which is done adaptively by looking at the stress in each cell; cells of largest stress and their immediate neighbors are selected as atomistic cells.

(ii) Solving the atomistic subproblem, as described above.

(iii) Evolving the macroscopic variables using the continuum equation in the continuum region and the empirically calculated elastic forces from the atomistic model in the atomistic region.

In this formulation, passage of the macroscopic data to the atomistic region is done naturally at the initialization step for the atomistic subproblem and at the macroscale evolution step.

6. APPLICATIONS

6.1. Dislocation Dynamics in the Frenkel–Kontorova Model

As the simplest model that encompasses most of the issues in a coupled atomistic–continuum simulation, we consider the Frenkel–Kontorova model

$$\ddot{x}_j = x_{j+1} - 2x_j + x_{j-1} - U'(x_j) + f, \tag{6.1}$$

where U is a periodic function with period 1 and f is an external forcing. The continuum limit of this equation is simply the Klein–Gordan equation

$$u_{tt} = u_{xx} - Ku + f, \tag{6.2}$$

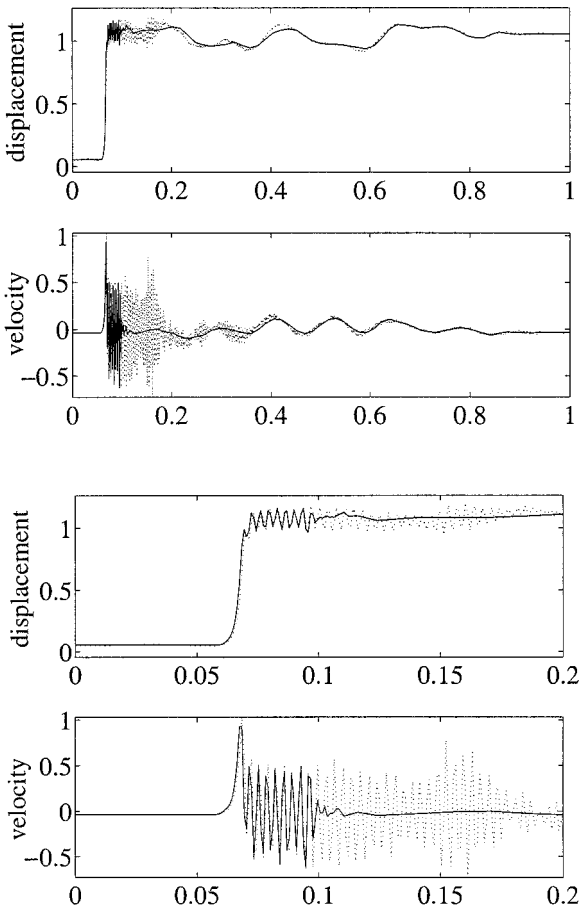

FIG. 7. Comparison of the displacement and velocity profiles computed using the full atomistic and the atomistic–continuum models, with $f = 0.04$. (Top two graphs) The results in the whole computational domain; (bottom two graphs) the details near the dislocation; (solid line) The result of the atomistic–continuum method; (dashed line) the result of the full atomistic method.

where $K = U''(0)$. We consider the case where there is a dislocation and study its dynamics under a constant applied forcing. In this example we take (6.1) as our atomistic model and (6.2) as our continuum model.

We first consider the case where a sharp transition is made between the atomistic and the continuum regions with a 1 : 16 ratio for the size of the grids. Figure 7 is a comparison of the displacement and velocity fields computed using the full atomistic model and the coupled atomistic–continuum model, with $f = 0.04$. The atomistic region has 32 atoms. The full atomistic simulation has 10^3. Dislocation appears as a kink in the displacement field. Notice that at the atomistic–continuum interface, there is still substantial phonon energy, which is then suppressed by the reflectionless boundary condition. No reflection of phonons back to the atomistic region is observed. In Fig. 8, we compare the positions of the dislocation as a function of time, computed using the coupled method and the detailed molecular dynamics. Extremely good agreement is observed.

We next consider a case with $f = 0.02$, which alone is too weak to move the dislocation. To the left of the dislocation, we add a sinusoidal wave to the initial data. The dislocation

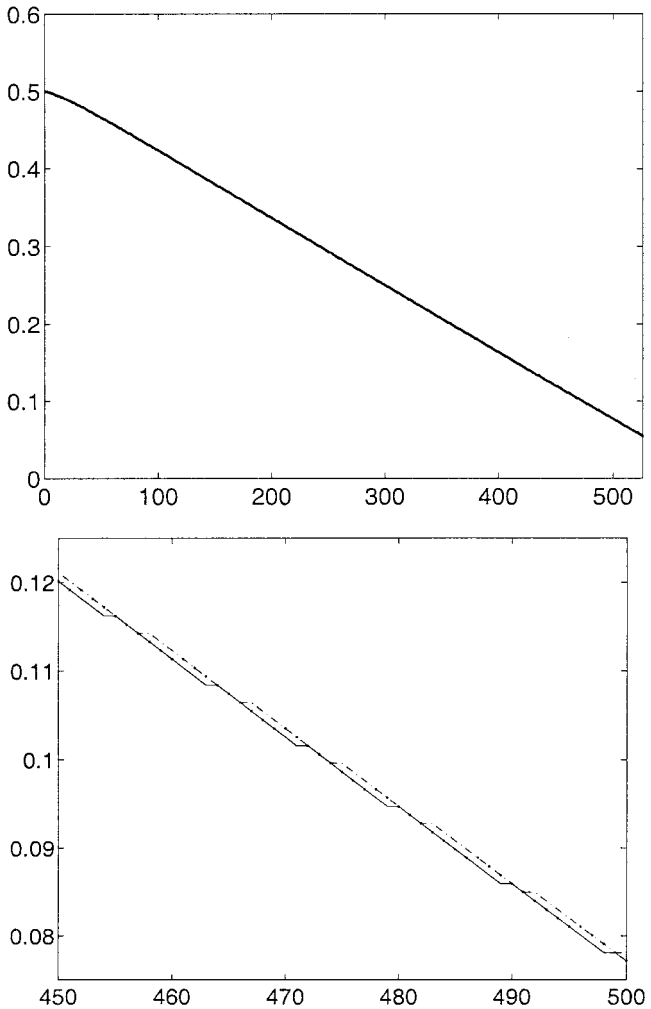

FIG. 8. Comparison of the positions of the dislocation as a function of time computed using the coupled method and the detailed molecular dynamics, with $f = 0.04$. (Dotted line) The result of the full MD simulation; (solid line) the result with gradual transition between atomistic and continuum regions; (dashed line) the result with a sharp transition.

moves as a consequence of the combined effect of the force and the interaction with the wave. Yet in this case the same atomistic–continuum method predicts an incorrect position for the dislocation, as shown in Fig. 9. The discrepancy seems to grow slowly in time (see Fig. 10). Improving the matching conditions does not seem to lead to significant improvement.

The difference between this case and the case shown in Fig. 7 is that there is substantially more energy at the intermediate scales. This is clearly shown in the energy spectrum that we computed for the two cases but it can also be seen in Fig. 9, where an appreciable amount of small scale waves are present in front of the dislocation. Such intermediate scales are suppressed in a method that uses a sharp transition between the atomistic and the continuum regions, unless we substantially increase the size of the atomistic region. We therefore consider the next alternative, in which the atomistic–continuum transition is made gradually in a 1 : 2 or 1 : 4 ratio between neighboring grids. In this way, the continuum

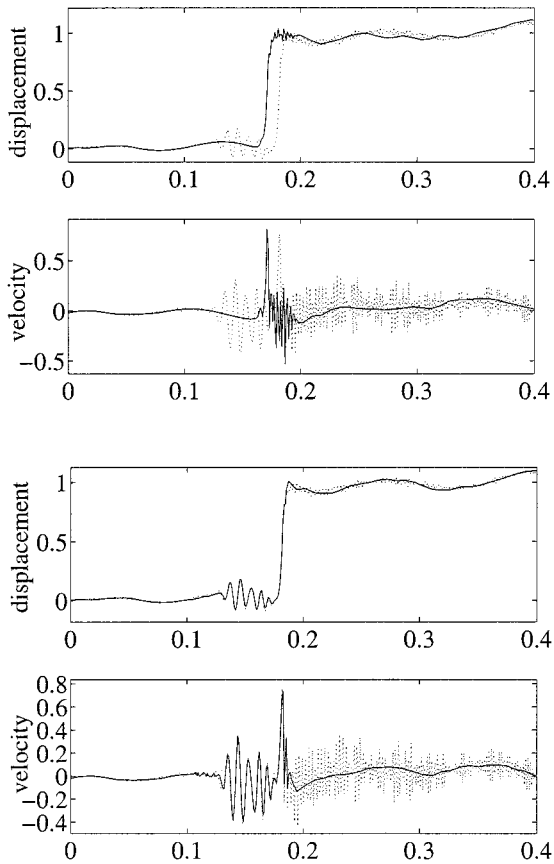

FIG. 9. Comparison of the displacement and velocity profiles computed using the full atomistic and the atomistic–continuum models, with $f = 0.02$. (Top two graphs) The results when the transition from the atomistic to the continuum region is sharp; (bottom two graphs) the results when the transition is gradual; (solid line) the result of the atomistic–continuum method; (dashed line) the result of the full atomistic method. Only the region near the dislocation is shown.

model in the transition region is able to capture the energy at the intermediate scales. The bottom two figures in Fig. 9 shows the results of such a method that uses a gradual $1:2$ transition. We see that the correct dislocation position is now recovered.

6.2. Friction between Flat and Rough Crystal Surfaces

Our second example is the friction between crystal surfaces. To model this process atomistically, we use standard molecular dynamics with the Lennard–Jones potential [15, 16]. First, we consider the case in which the two crystals are separated by a horizontal atomically flat interface. The atoms in the bottom crystal are assumed to be much heavier (by a factor of 10) than the atoms on top. To model the lack of chemical bonding between the atoms in the top and bottom crystals, the interaction forces are reduced by a factor of 5 between atoms in the top and bottom crystals. A constant shear stress is applied near the top surface. We use the periodic boundary condition in the x-direction.

From a physical viewpoint, one interesting issue here is how dissipation takes place. Physically the kinetic energy of the small scales appears as phonons, which then convert into

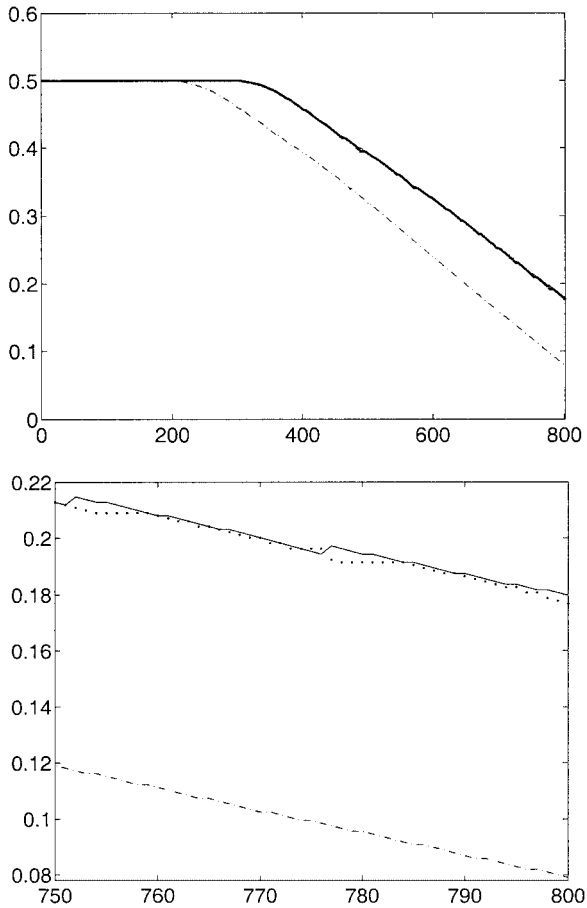

FIG. 10. Comparison of the positions of the dislocation as a function of time computed using the coupled method and the detailed molecular dynamics, with $f = 0.02$. (Dotted line) The result of the full MD simulation; (solid line) the result with a gradual transition between the atomistic and the continuum regions; (dashed line) the result with a sharp transition.

heat and exit the system. A standard practice in modeling such a process is to add a friction term to the molecular dynamics in order to control the temperature of the system [15, 16]. In contrast, we ensure the proper dissipation of phonons to the environment by imposing the reflectionless boundary conditions for the phonons. The results presented below are computed using the last set of coefficient matrices presented at the end of Section 4.

From Fig. 11 we see that we indeed obtain a linear relation between the mean displacement of the atoms in the top crystal as a function of time. The temperature of the system also reaches saturatation. Also plotted in Fig. 11 is the result of the mean displacement computed using the combined atomistic–continuum method. Here the continuum model is the linear elastic wave equation with Lame coefficients computed from the Lennard–Jones potential. The agreement between the full atomistic and the atomistic–continuum simulation is quite satisfactory.

Next, we study the friction between two rough crystal surfaces. The setup is the same as before, except that the initial interface between the crystals takes the form $y = f(x)$. The numerical results obtained are displayed in Fig. 12. In Fig. 13, we plot the positions of

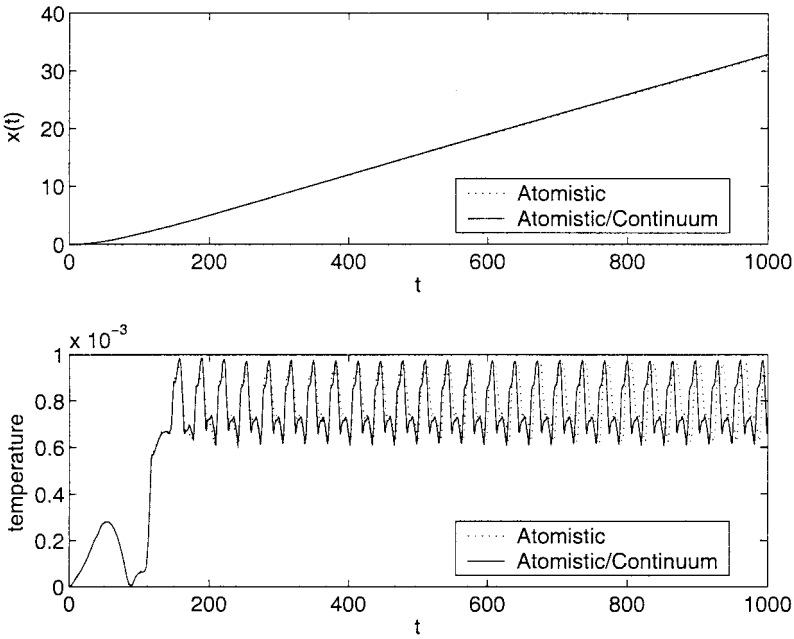

FIG. 11. Displacement and temperature as a function of time for the friction problem.

the atoms in the top and bottom crystals. We see that gaps are created in the case of rough interfaces.

In Fig. 14, we compare the force–velocity relations for both flat and rough interfaces. Again the agreement between the coupled method and the full atomistic method is quite good.

In the present problem, we used an atomistic model in a narrow strip near the interface and a continuum model away from the interface. An interesting question is how wide the

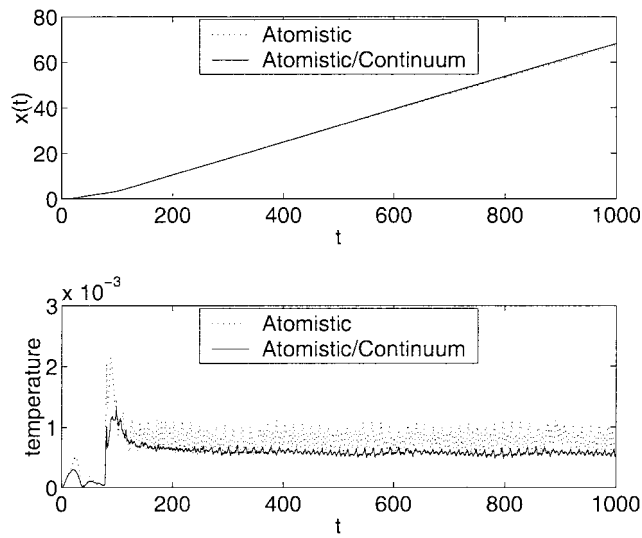

FIG. 12. Displacement and temperature as a function of time for friction between rough surfaces.

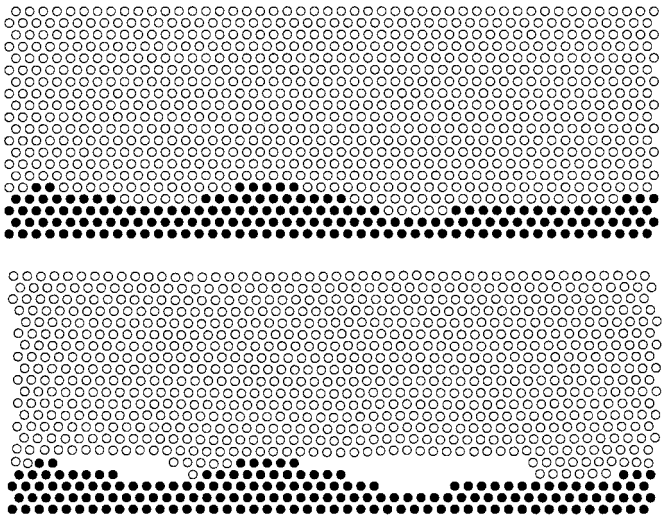

FIG. 13. The positions of the atoms near the interfaces. (White circles) Light atoms; (black ones) heavy atoms; (top graph) the initial state; (bottom graph) the late state at $t = 1000$.

atomistic strip has to be. Clearly, for the purpose of computational efficiency, we want the atomistic strip to be as narrow as possible. On the other hand, it has to be wide enough to provide an accurate description inside the boundary layer, where important atomistic processes can be relaxed. There are two important atomistic processes in the present problem. The first is the vibration of the atoms around their local equilibrium positions. The second is the process of moving from one local equilibrium to the next, i.e., sliding by one atomic distance. Clearly the second process works on a longer time scale. This process has to be resolved by the atomistic layer. In Fig. 15, we compare the atomic positions of a column of a atoms which were initially vertical; i.e., they had the same x-coordinates. From

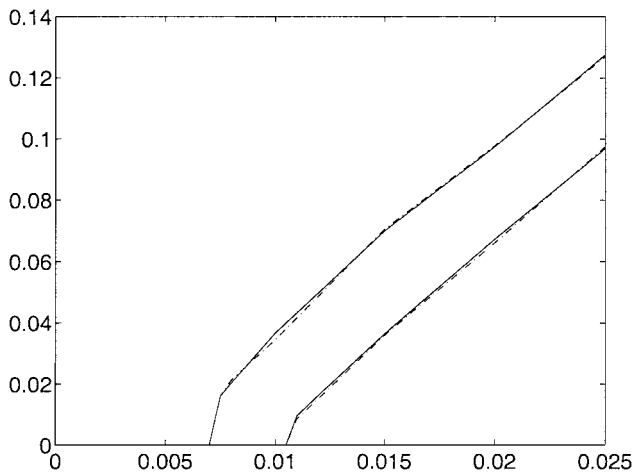

FIG. 14. Comparison of the force–velocity relations for both flat and rough interfaces. (Upper) The results for a flat case; (lower lines) the results for a rough case; (solid lines) the results for the coupled atomistic–continuum method; (dashed lines) the results for the full MD simulation.

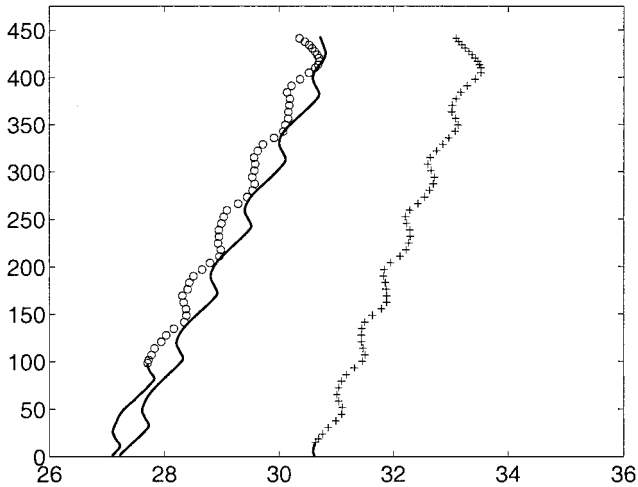

FIG. 15. Comparison of the atomic positions of a column of atoms which had the same x-coordinates initially. (Solid line) The result of the full MD simulation; (open circles) the result of the coupled method with 96 layers in the atomistic region; (crosses) the result of the coupled method with 16 layers in the atomistic region. In the coupled method, the ratio of atomistic to continuum grids was 1 : 8.

this picture one can also estimate the strain rate. We can clearly see that if the atomistic layer does not resolve the phonons generated by the second process, we get inaccurate results.

6.3. Crack Propagation

Our third example is the Slepyan model of fracture dynamics (2.11). In our coupled atomistic–continuum method, we use full atomistic simulation (2.11) around the crack tip, and we use (2.12) in the region away from the crack tip. For the continuum equation, we use the displacement boundary condition $u_{\pm} = {}_{\pm}U_N$ at the left boundary and the stress boundary condition $\frac{\partial u}{\partial x} = 0$ at the right boundary. Figure 16 is a comparison of the fracture

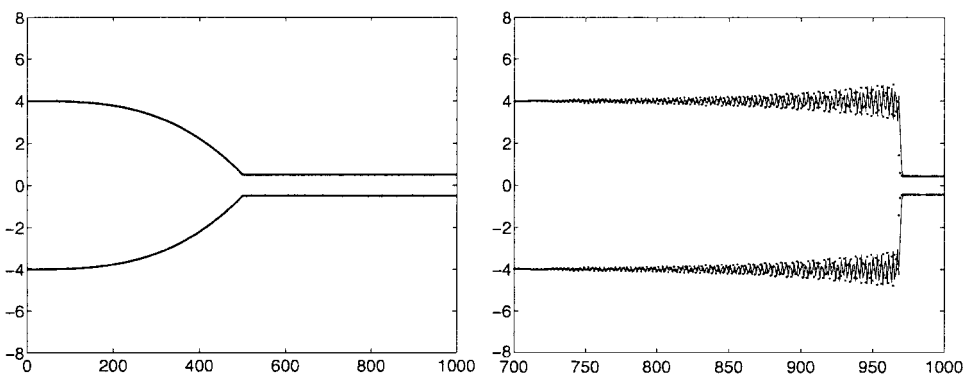

FIG. 16. One-dimensional fracture problem. (Left) The fracture surface at time $t = 0$; (right) the fracture surface at time $t = 600$ with $b = 0.01$, $N = U_N = 4$; (Dashed line) The result of the molecular dynamics simulation; (solid line) the result of the coupled atomistic–continuum method. The ratio of atomistic to continuum grids was 1 : 8.

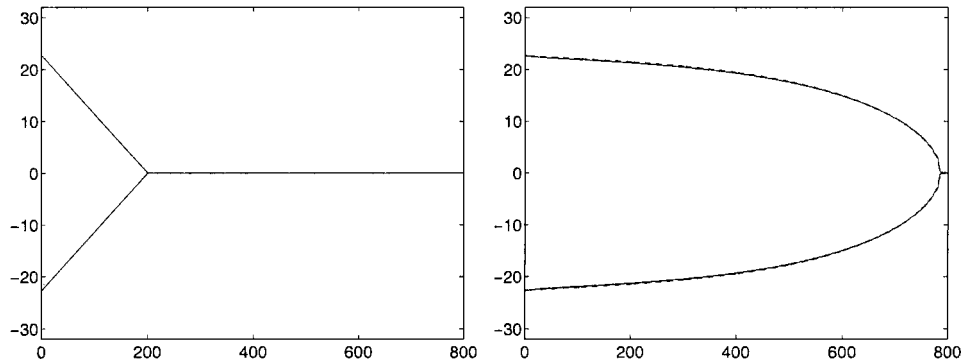

FIG. 17. Two-dimensional fracture problem. (Left) The fracture surface at time $t = 0$; (right) the fracture surface at time $t = 200$ with $b = 0.01$, $N = 512$, and $U_N = \sqrt{N}$. There are 800 atoms in each row. (Dashed line) The result of the full molecular dynamics simulation; (solid line) the result of the coupled atomistic–continuum method. In the coupled method, we divided the whole domain into three parts: the middle, including the crack surface with 800×64 atoms, is the MD region; the top and bottom are continuum regions. The ratio of atomistic to continuum grids in each dimension was 1 : 8.

surface computed using the full atomistic model and the coupled atomistic–continuum method.

Next we apply our method to the 2D Mode III fracture dynamics on a square lattice (2.14). The same boundary conditions as in the 1D case are used for the continuum model. For the matching conditions between the atomistic and the continuum regions, we used a stencil that consists of seven points: the values of the three nearest grid points next to the boundary at the current and previous time steps, plus the value at the boundary grid point at the previous time step. The optimization is carried out using angles $\theta = 45^\circ, 90^\circ, 135^\circ$. Figure 17 is a comparison of the fracture surface computed using the full atomistic model and the coupled atomistic–continuum method. Comparisons of the positions of the fracture

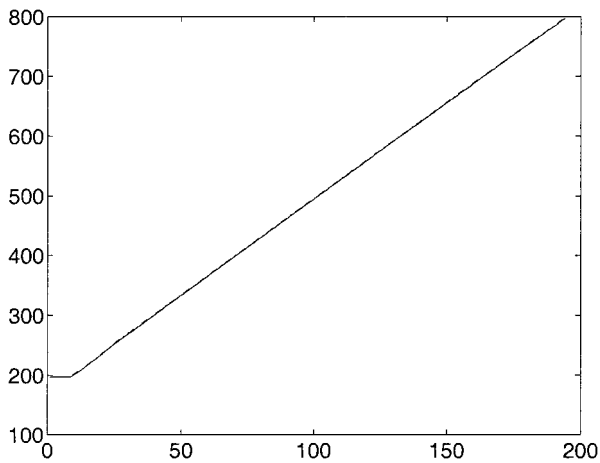

FIG. 18. Comparisons of the positions of the crack tip as a function of time. (Dashed line) The result of the full MD simulation; (solid line) the result of the coupled method.

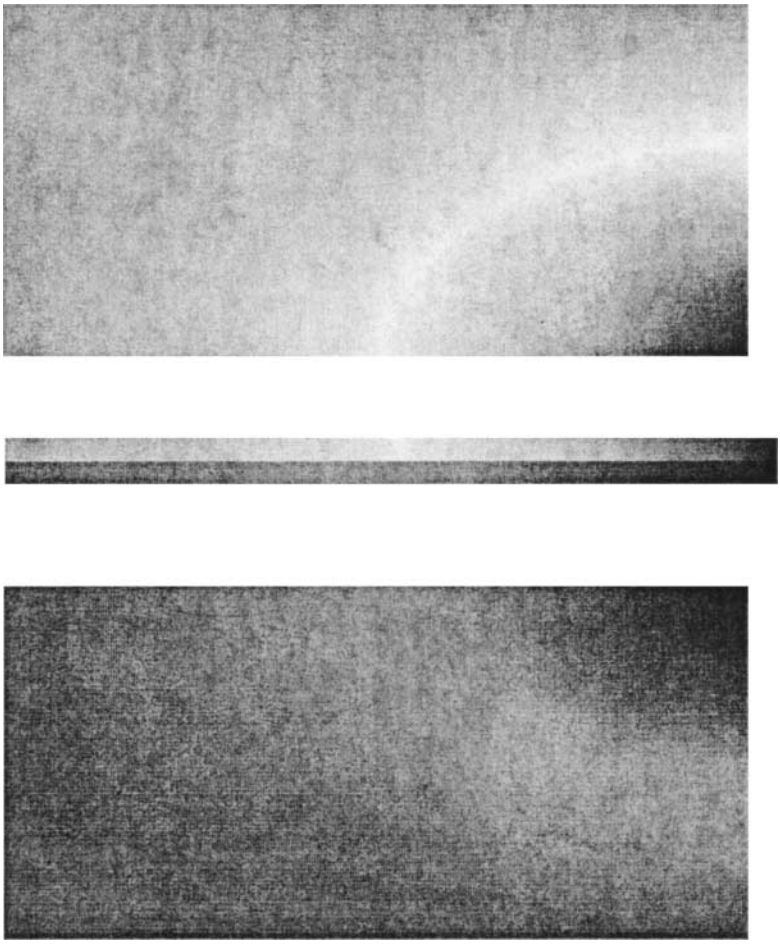

FIG. 19. The shear waves. We divided the whole domain with 2048×2048 atoms into three parts: the middle, including the crack surface with 2048×128 atoms, is the MD region; the top and bottom are continuum regions with 128×62 finite difference grids in each region.

tip as a function of time is given in Fig. 18. The results are quite satisfactory. In Fig. 19, we display the shear waves generated as a result of the crack propagation, No reflection is seen. In Fig. 20, we show an enlarged picture of the molecular dynamics region near the crack tip.

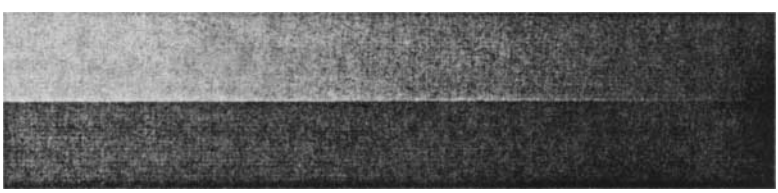

FIG. 20. The enlarged picture of the MD region near the crack tip.

7. CONCLUSION

In conclusion, we presented a new strategy for the matching conditions at the atomistic–continuum interface in multiscale modeling of crystals. The main idea is to choose the boundary condition by minimizing the reflection of phonons along a few low-symmetry atomic planes, subject to some accuracy constraints at low wavenumbers. These conditions are adaptive if we choose the weight functions in (4.20) and (4.31) to reflect the evolving nature of the small scales. They minimize the reflection of phonons and at the same time ensure accurate passage of large-scale information. The coupled atomistic–continuum method presented here is quite robust and works well at low temperature. At finite temperature and when nonlinearity is important at large scales, a new method must be worked out. This work is in progress. Also of interest is coarse graining in time. This can be done naturally in the present framework by restricting the duration of the atomistic subproblem solved at each macro step to only a small protion of Δt and estimating the needed macroscale data from this restricted data set. This is carried out in [23].

Perhaps the most significant restriction of the present algorithm is that of low temperature. At finite temperature, phonons contribute to the dynamics of the system at both macro- and microscales. The matching condition at the atomistic–continuum interface should not just be the dissipation of phonons. Rather it should model accurately the exchange of heat between the atomistic region and the environment. This again is work in progress.

ACKNOWLEDGMENTS

We thank Tim Kaxiras for suggesting the problem of friction between rough interfaces. This work is supported in part by NSF through a PECASE award and by ONR Grant N00014-01-1-0674.

REFERENCES

1. E. B. Tadmor, M. Ortiz, and R. Phillips, Quasicontinuum analysis of defects in crystals, *Philos. Mag.* **A73**, 1529 (1996).
2. V. B. Shenoy, R. Miller, E. B. Tadmor, D. Rodney, R. Phillips, and M. Ortiz, An adaptive finite element approach to atomic-scale mechanics—the quasicontinuum method, *J. Mech. Phys. Solids* **47**, 611 (1999).
3. F. F. Abraham, J. Q. Broughton, N. Bernstein, and E. Kaxiras, Concurrent coupling of length scales: Methodology and application, *Phys. Rev. B* **60**(4), 2391 (1999).
4. F. F. Abraham, J. Q. Broughton, N. Bernstein, and E. Kaxiras, Spanning the continuum to quantum length scales in a dynamic simulation of brittle fracture, *Europhys. Lett.* **44**(6), 783 (1998).
5. R. E. Rudd and J. Q. Broughton, Atomistic simulation of MEMS resonators through the coupling of length scales, *J. Modeling Simulation Microsystems* **1**(1), 29 (1999).
6. R. E. Rudd and J. Q. Broughton, Coarse-grained molecular dynamics and the atomic limit of finite elements, *Phys. Rev. B* **58**(10), R5893 (1998).
7. W. Cai, M. de Koning, V. V. Bulatov, and S. Yip, Minimizing boundary reflections in coupled-domain simulations, *Phys. Rev. Lett.* **85**(15), 3213 (2000).
8. V. B. Shenoy, R. Miller, E. B. Tadmor, *et al*., Quasicontinuum models of interfacial structure and deformation, *Phys. Rev. Lett*. **80**(4), 742 (1998).
9. R. Miller, E. B. Tadmor, R. Phillips, *et al*., Quasicontinuum simulation of fracture at the atomic scale, *Model Simul. Mater. Sci.* **6**(5), 607 (1998).
10. G. S. Smith, E. B. Tadmor, and E. Kaxiras, Multiscale simulation of loading and electrical resistance in silicon nanoindentation, *Phys. Rev. Lett.* **84**(6), 1260 (2000).

11. W. E and Z. Huang, Matching conditions in atomistic-continuum modeling of materials, *Phys. Rev. Lett.* **87**(13), 135501 (2001).
12. M. Ehrhardt and A. Arnold, Discrete transparent boundary conditions for the Schrödinger equation, *Rev. Mat. Univ. Parma* **6/4**, 57–108 (2001).
13. R. Clayton and B. Engquist, Absorbing boundary conditions for acoustic and elastic wave equations, *Bull. Seismol. Soc. Ame.* **67**(6), 1529 (1977).
14. B. Engquist and A. Majda, Radiation boundary conditions for acoustic and elastic wave calculations, *Commun. Pure Appl. Math.* **32**, 313 (1979).
15. J. A. Harrison and D. W. Brenner, Atomic-scale simulation of tribological and related phenomena, in Handbook of Micro/Nano Tribology, edited by B. Bhushan (CRC Press, Boca Raton, FL, 1995).
16. M. O. Robbins and M. H. Müser, Computer simulations of friction, lubrication and wear, in *Modern Tribology Handbook*, edited by B. Bhushan (CRC Press, Boca Raton, FL, 2001).
17. M. Marder and S. Gross, Origin of crack tip instabilities, *J. Mech. Phys. Solids* **43**(1), 1 (1995).
18. W. E and Z. Huang, Multiscale modeling of friction between crystal surfaces, manuscript in preparation.
19. M. Berger and J. Oliger, Adaptive mesh refinement for hyperbolic partical differential equations, *J. Comput. Phys.* **53**, 484 (1984).
20. W. G. Szymczak and I. Babuska, Adaptivity and error estimation for the finite-element method applied to convection-diffusion problems, *SIAM J. Numer. Anal.* **21**(5), 910 (1984).
21. A. Safjan, L. Demkowicz, and J. T. Oden, Adaptive finite-element methods for hyperbolic systems with application to transient acoustics, *Int. J. Numer. Methods Eng.* **32**(4), 677 (1991).
22. W. Bangerth and R. Rannacher, Adaptive finite-element techniques for the acoustic wave equation, *J. Comput. Acoust.* **9**(2), 575 (2001).
23. W. E, B. Engquist and Z. Huang, *The Heterogeneous Multi-Scale Method—A General Methodology for Multi-Scale Modeling*, preprint (2002).